Analysis and optimization of multi-branch interconnect architecture based on multi-port transfer matrix

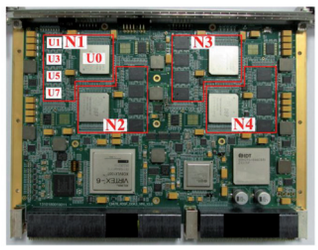

Análisis y optimización de la arquitectura de interconexión multi-ramales basada en la matriz de transferencia multi-puerto

Xingming Li[1*], Shanqing Hu[2] and Junwei Zhang[3]

[1] Tsinghua University, Shuangqing Road 30#, Haidian District, 100084, Beijing, China. * Corresponding author, email: lxm11544@163.com .
[2] Beijing Institute of Technology, Zhongguancun South Street 9#, Haidian District, 100081, Beijing, China.
[3] Nanyang Technological University, 50 Nanyang Avenue, 639798, Singapore.

DOI: https://doi.org/10.6036/8360 | Recibido: 21/03/2017 • Evaluado: 21/03/2017 • Aceptado: 27/04/2017

RESUMEN

• La arquitectura de interconexión multi-ramales (MBIA) es una forma eficaz de lograr sistemas eléctricos de muy alta velocidad y muy alta integración. Sin embargo, la creciente frecuencia y complejidad de funcionamiento provocan cuestiones criticas de integridad de la señal (SI). La mayoría de los estudios existentes se centran en el modelado y el análisis de la propia arquitectura, pero ignoran los correspondientes efectos de terminación de línea, lo que resulta en un análisis inexacto y una optimización ineficaz. Para analizar y optimizar el MBIA con precisión y efectividad, el presente estudio propuso una matriz de transferencia de multi-puerto (MPTM) que tuvo en cuenta los efectos de terminación, y también se desarrolló una estrategia híbrida de dominio tiempo-frecuencia basada en MPTM. En primer lugar, MBIA fue modelado como dos redes multi-puerto generalizadas en cascada que respectivamente representan MBIA y sus terminaciones. En segundo lugar, se definió MPTM y se derivó la estrategia basada en MPTM. Por último, se demostró el principio y el desempeño de las estrategias propuestas mediante una interconexión de ocho direcciones DDR3 de topología fly-by con una velocidad de línea de hasta 667 Mbps. Los resultados de la simulación verifican que el MPTM propuesto representa un MBIA completo considerando los efectos de terminación y proporciona un sesgo efectivo para el análisis y la optimización. Al emplear la estrategia basada en MPTF, la altura del ojo de la señal de dirección DDR3 en el caso de estudio alcanza una tasa de crecimiento promedio del 80%frente al diseño original. Los resultados obtenidos en este estudio pueden ser aplicados para obtener el rendimiento óptimo y la estabilidad de los sistemas eléctricos que implican MBIA.

• **Palabras clave:** Interconexión de múltiples ramas, multipuerto, función de transferencia, matriz de dispersión, efectos de terminación.

ABSTRACT

Multi-branch interconnect architecture (MBIA) is an effective way to achieve ultra-high-speed and ultra-high-integration electrical systems. However, the increasing frequency and complexity of operation result in critical signal integrity (SI) issues. The majority of existing studies focuses on modeling and analyzing the architecture itself but ignores corresponding termination effects thereby resulting in inaccurate analysis and ineffective optimization. To analyze and optimize MBIA accurately and effectively, the present study proposed a multi-port transfer matrix (MPTM) that considered termination effects into account, and a hybrid time-frequency domain strategy based on MPTM was also developed. First, MBIA was modeled as two cascaded generalized multi-port networks that respectively represented MBIA and its terminations. Second, MPTM was defined and MPTM-based strategy was derived. Finally, the principle and performance of the proposed strategies were demonstrated through an eight-DDR3 address interconnect of fly-by topology with a line rate of up to 667 Mbps. The simulation results verifies that the proposed MPTM represents a complete MBIA by considering termination effects and provides effective bias for analysis and optimization. According to the MPTF-based analysis and optimization strategy, by adding a specific capacitor near the transmitter output, the simulated eye height of the address signal attains an average growth rate of 80% of the original design, and this optimaizaiton aslo achieves steady performance in real projects. The results obtained in this study can be applied to obtain the optimal performance and stability of electrical systems involving MBIA.

Keywords: Multi-branch interconnect, multi-port, transfer function,scattering matrix, termination effects.

1. INTRODUCTION

Given the imperious demand for ultra-high performance electrical systems, multi-branch interconnect architecture (MBIA) is widely used to integrate an increasing number of integrated circuits (ICs). However, increasing speed and density of MBIA result in critical signal integrity (SI) issues, which may cause faulty system switch or logic errors and design iterations [1]. Collective factors influence SI issues. One of these factors is pronounced transmission effects, such as dispersion, propagation delay, and coupling; these may cause amplitude attenuation, timing conflict, crosstalk [2–3]. Another factor is complicated reflection that become prominent influencing factor because of discontinuities, such as transition, branches, and terminations; these discontinuities may cause overshoot, undershoot, ringing, and resonances [4]. These factors have standalone and mutual influences that increase the complexity and difficulty of obtaining the optimal performance and stability of electrical systems that involve MBIA.

A number of traditional studies were conducted to solve these issues. Valuable progress has been achieved, but limitations continue to exist. Most of these studies focus on modeling and characterizing isolated or combined non-ideal effects by lacking termination effects thereby resulting in incomplete systemic characterization. Besides, analysis and optimization are performed in the

frequency or time domain and rarely in the hybrid time–frequency domain thereby resulting in inaccurate analysis and ineffective optimization. Thus, unwanted design iterations may be conducted, which entails long development cycles and increased cost. Moreover, performance margins may deteriorate, which threatens optimal performance and long-term stability.

Hence, MBIA should be characterized and modeled accurately by considering comprehensive non-ideal effects. Meanwhile, an effective strategy that employs hybrid time–frequency domain analysis and optimization is required to achieve optimal design. This study proposes a multi-port transfer matrix (MPTM) to analyze MBIA by introducing the concept of transfer function. MPTM can characterize system structures, including termination effects in the frequency domain, and can identify the root cause of SI problems and offer accurate bias for optimization. Time-domain waveforms can be predicted with the aid of fast Fourier transform (FFT) and inverse fast Fourier transform (IFFT) to offer performance assessment. By combining the frequency-domain analysis and time-domain assessment, the electrical systems involving MBIA can be finally optimized through what-if iterations.

2. STATE OF THE ART

Electrical systems involving MBIA are attracting worldwide attention from researchers and companies; a number of achievements were obtained, which included modeling of MBIA and proposing methods for analysis and optimization [5–9]. In [5], the authors proposed a novel model for uniform or non-uniform multi-conductor transmission line based on scattering matrix (S-matrix); this transmission line represented high-speed interconnect as a multiple-input multiple-output (MIMO) channel. The author proposed a linear pre-coding scheme to avoid crosstalk effects. In [6], the authors proposed an efficient signal integrity analysis and optimization method for complicated MIMO networks based on S-matrix models; data mining was employed to save significant analysis time and improve efficiency. In [7], the authors proposed an innovative analysis of network (TAN) model of asymmetrical 1:2 Y-tree interconnects. The model of the two-level Y-tree system was analytically established through the equivalent Z-matrix and the corresponding equivalent S-parameters. In [8], the authors investigated and compared two simulation models of lossy transmission lines for signal integrity analysis, including the SPICE model obtained by applying the vector fitting technique and the S-parameter model based on behavioral modeling technique and time-domain convolution. In [9], the authors proposed an estimation method for the S-matrix to characterize multiport connections and devices by solving linear and quadratic equations. Most of these achievements used S-matrix to model, analyze, and optimize the overall link path through full-wave EM methods [10], such as the method of moments [11], finite-difference time-domain method [12], finite element method [13] and vector fitting [14]. However, S-matrix is defined under the condition that the related ports are terminated with characteristic impedance of commonly 50 ohm, and this will result in the infeasibility of characterizing practical electrical systems by including termination effects. Moreover, the S-matrix is related to incident and reflected waves, which are not compatible to the termination of electrical specifications.

Since transfer function has no termination requirements and is related to the input and output synthesized signals (voltage or current) it offers a solution for overcoming the limitations of S-matrix-based methods and has been adopted in a number of studies. In [15], the authors employed the transfer function to study the discontinuities of interconnects to anticipate electromagnetic interference problems. In [16], the authors adopted the transfer function to eliminate differential signaling data error caused by external energy in long cables. In [17], the authors investigated coupled interconnects to identify SI problems based on transfer function; they proposed de-embedding techniques to compensate channel errors. In [18], the authors presented a method for estimating the electromechanical damping and frequency coefficients of interconnected power systems by introducing transfer function. The proposed method required time-reduced computations and was demonstrated as feasible. In [19] and [20], the authors proposed approximate closed-form transfer function model for diverse single and differential interconnects; the model was accurate and could achieve time-reduced computation. However, these methods mainly employed transfer function to model isolated interconnects or link path and rarely considered termination effects, and did not introduce the concept to MBIA.

The remainder of this study is organized as follows. Section 3 describes the derivation of MPTM and presents the MPTM-based strategy for analysis and optimization. Section 4 demonstrates the proposed strategies through an eight-DDR3 address interconnect of fly-by topology with a line rate of up to 667 Mbps. Section 5 provides the conclusions.

3. METHODOLOGY

3.1. GENERALIZED NETWORK MODEL OF MBIA

Fig. 1 (see section: supplementary material) shows a typical electrical system involving MBIA with a single transmitter and N receivers. V_T and I_T denote the voltage and current of the transmitter output, and V_1–V_N and I_1–I_N denote those at the receiver (R_1–R_N) input. The link path of the MBIA is a combination of transmission lines, vias, and branches, whereas the receivers are composed of its terminations.

A complete MBIA is represented as a multi-port network called N_C, as illustrated in Fig. 2. The network is generalized as two cascaded networks, namely, network N_A and network N_B. N_A represents the link-path network that connects the transmitter and receivers. This N+1 port network has a single input and N outputs. A_T and A_n denote the input (transmitter port) and the nth output (nth receiver port), respectively.

To adopt subsequent derivations, S-matrix S_A of link-path network N_A is divided into four sub-matrices expressed as:

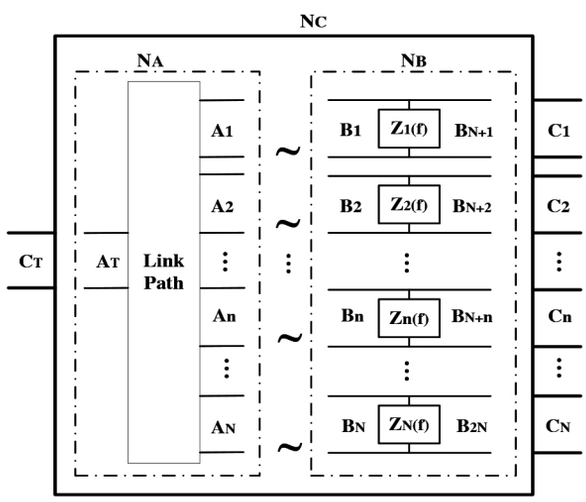

Fig. 2. Generalized complete network model of a multi-branch interconnect architecture

$$S_A = \begin{bmatrix} \overbrace{\begin{pmatrix} S_{11} & \cdots & S_{1N} \\ \vdots & \ddots & \vdots \\ S_{N1} & \cdots & S_{NN} \end{pmatrix}}^{S_A^{(I,I)}} & \overbrace{\begin{pmatrix} S_{1T} \\ \vdots \\ S_{NT} \end{pmatrix}}^{S_A^{(I,II)}} \\ \underbrace{\begin{pmatrix} S_{T1} & \cdots & S_{TN} \end{pmatrix}}_{S_A^{(II,I)}} & \underbrace{\begin{pmatrix} S_{TT} \end{pmatrix}}_{S_A^{(II,II)}} \end{bmatrix} \quad (1)$$

In this N+1 port network, A_T is the (N+1)th port, whereas A_n is the nth port.

N_B represents a termination network that involves N receivers. This 2N port network has N input (B_1–B_N) and N output (B_{N+1}–B_{2N}). N_B comprises N independent two-port networks, where B_n and B_{N+n} are the input and output ports, respectively, of the nth network. Impedance $Z_n(f)$ (looking into the receiver) can be obtained from measurements or extracted from equivalent circuits based on SPICE or IBIS models as illustrated in Fig. 3(a) (see section: supplementary material). C_{pkg}, L_{pkg}, and R_{pkg} denote package capacitance, inductance, and resistance, respectively, whereas C_{comp} denotes on-die capacitance.

Impedance $Z_n(f)$ of the nth two-port network in Fig. 3(b) (see section: supplementary material) can be calculated as:

$$Z_n(f) = \frac{Z_{C_{pkg}} * \left(Z_{L_{pkg}} + Z_{R_{pkg}} + Z_{C_{comp}}\right)}{Z_{C_{pkg}} + Z_{L_{pkg}} + Z_{R_{pkg}} + Z_{C_{comp}}} \quad (2)$$

where the elements are related to angular frequency ω as

$$\begin{cases} Z_{C_{pkg}} = 1/\, j\omega C_{pkg} \\ Z_{L_{pkg}} = j\omega L_{pkg} \\ Z_{R_{pkg}} = R_{pkg} \\ Z_{C_{comp}} = 1/\, j\omega C_{comp} \end{cases} \quad (3)$$

The S-matrix S_n of the nth two-port network can be calculated as:

$$S_n = \begin{pmatrix} \Gamma_n & 1+\Gamma_n \\ 1+\Gamma_n & \Gamma_n \end{pmatrix} \quad (4)$$

where Γ_n is the reflection coefficient given by:

$$\Gamma_n = \frac{Z_0 \,\|\, Z_n(f) - Z_0}{Z_0 \,\|\, Z_n(f) + Z_0} = \frac{-Z_0}{2Z_n(f) + Z_0} \quad (5)$$

where Z_0 denotes characteristic impedance. By combining N independent two-port networks and using Eq. 5, the S-matrix S_B of termination network N_B is given by

$$S_B = \begin{bmatrix} \overbrace{\begin{pmatrix} \Gamma_1 & \cdots & 0 \\ \vdots & \ddots & \vdots \\ 0 & \cdots & \Gamma_N \end{pmatrix}}^{S_B^{(I,I)}} & \overbrace{\begin{pmatrix} 1+\Gamma_1 & \cdots & 0 \\ \vdots & \ddots & \vdots \\ 0 & \cdots & 1+\Gamma_N \end{pmatrix}}^{S_B^{(I,II)}} \\ \underbrace{\begin{pmatrix} 1+\Gamma_1 & \cdots & 0 \\ \vdots & \ddots & \vdots \\ 0 & \cdots & 1+\Gamma_N \end{pmatrix}}_{S_B^{(II,I)}} & \underbrace{\begin{pmatrix} \Gamma_1 & \cdots & 0 \\ \vdots & \ddots & \vdots \\ 0 & \cdots & \Gamma_N \end{pmatrix}}_{S_B^{(II,II)}} \end{bmatrix} \quad (6)$$

where S_B is divided into four sub-matrices to adopt the subsequent derivations.

3.2. CASCADING OF MULTI-PORT SCATTERING MATRIX

The cascading algorithm of the two multi-port networks is derived first as a prerequisite of the proposed MPTM . In Fig. 4, multi-port network N_Z is represented by cascading two multi-port networks N_X and N_Y with a k-to-k junction. N_X is an m-port network with m-k input (X_{k+1}–X_m) and k output (X_1–X_k), and is represented by S_X. N_Y is an n-port network with k input (Y_1–Y_k) and n-k output (Y_{k+1}–Y_n), and is represented by S_Y. By cascading N_X and N_Y, we obtain N_Z as an m+n-2k port network with m-k input (Z_1–Z_{m-k}) and n-k output (Z_{m-k+1}–Z_{m+n-2k}).

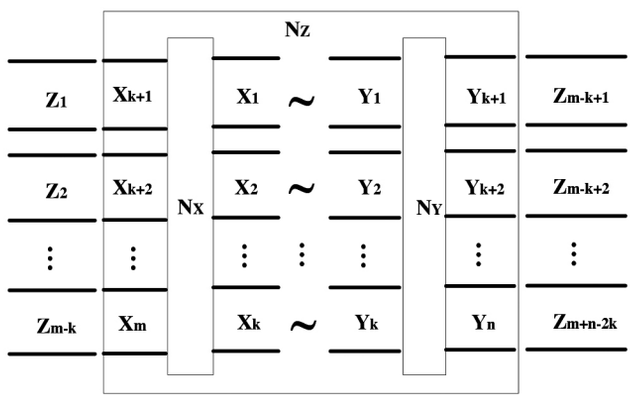

Fig. 4. Cascading of m-port network N_X and n-port network N_Y with a k-to-k junction

Matrices S_X and S_Y can be divided into four sub-matrices according to the distribution of input and output:

$$S_X = \begin{bmatrix} \overbrace{\begin{pmatrix} Sx_{1,1} & \cdots & Sx_{1,k} \\ \vdots & \ddots & \vdots \\ Sx_{k,1} & \cdots & Sx_{k,k} \end{pmatrix}}^{S_X^{(I,I)}} & \overbrace{\begin{pmatrix} Sx_{1,k+1} & \cdots & Sx_{1,m} \\ \vdots & \ddots & \vdots \\ Sx_{k,k+1} & \cdots & Sx_{k,m} \end{pmatrix}}^{S_X^{(I,II)}} \\ \underbrace{\begin{pmatrix} Sx_{k+1,1} & \cdots & Sx_{k+1,k} \\ \vdots & \ddots & \vdots \\ Sx_{m,1} & \cdots & SX_{m,k} \end{pmatrix}}_{S_X^{(II,I)}} & \underbrace{\begin{pmatrix} Sx_{k+1,k+1} & \cdots & Sx_{k+1,m} \\ \vdots & \ddots & \vdots \\ Sx_{m,k+1} & \cdots & Sx_{m,m} \end{pmatrix}}_{S_X^{(II,II)}} \end{bmatrix} \quad (7)$$

$$S_Y = \begin{bmatrix} \overbrace{\begin{pmatrix} Sy_{1,1} & \cdots & Sy_{1,k} \\ \vdots & \ddots & \vdots \\ Sy_{k,1} & \cdots & Sy_{k,k} \end{pmatrix}}^{S_Y^{(I,I)}} & \overbrace{\begin{pmatrix} Sy_{1,k+1} & \cdots & Sy_{1,m} \\ \vdots & \ddots & \vdots \\ Sy_{k,k+1} & \cdots & Sy_{k,m} \end{pmatrix}}^{S_Y^{(I,II)}} \\ \underbrace{\begin{pmatrix} Sy_{k+1,1} & \cdots & Sy_{k+1,k} \\ \vdots & \ddots & \vdots \\ Sy_{m,1} & \cdots & Sy_{m,k} \end{pmatrix}}_{S_Y^{(II,I)}} & \underbrace{\begin{pmatrix} Sy_{k+1,k+1} & \cdots & Sy_{k+1,m} \\ \vdots & \ddots & \vdots \\ Sy_{m,k+1} & \cdots & Sy_{m,m} \end{pmatrix}}_{S_Y^{(II,II)}} \end{bmatrix} \quad (8)$$

Based on Eqs. 7 and 8, the sub-matrices of S_Z can be written as:

$$S_Z(I,I) = S_X(II,I)S_Y(I,I)(\Delta S)S_X(I,II) + S_X(II,II) \quad (9)$$

$$S_Z(I,II) = S_X(II,I)S_Y(I,I)(\Delta S)S_X(I,I)S_Y(I,II) + S_X(II,I)S_Y(I,II) \quad (10)$$

$$S_Z(II,I) = S_Y(II,I)(\Delta S)S_X(I,II) \quad (11)$$

$$S_Z(II,II)=S_Y(II,I)(\Delta S)S_X(I,I)S_Y(I,II)+S_Y(II,II) \quad (12)$$

where $\Delta S=\left(U_k-S_X(I,I)S_Y(I,I)\right)^{-1}$ and U_k is a k x k unit matrix. In Eqs. 9 to 12, S_Z, which characterizes network N_Z, is given as:

$$S_Z=\begin{bmatrix} S_Z(I,I) & S_Z(I,II) \\ S_Z(II,I) & S_Z(II,II) \end{bmatrix} \quad (13)$$

where the four sub-matrices are given by

$$S_Z(I,I)=\begin{pmatrix} S_{1,1} & \cdots & S_{1,m-k} \\ \vdots & \ddots & \vdots \\ S_{m-k,1} & \cdots & S_{m-k,m-k} \end{pmatrix} \quad (14)$$

$$S_Z(I,II)=\begin{pmatrix} S_{1,m-k+1} & \cdots & S_{1,m+n-2k} \\ \vdots & \ddots & \vdots \\ S_{m-k,m-k+1} & \cdots & S_{m-k,m+n-2k} \end{pmatrix} \quad (15)$$

$$S_Z(II,I)=\begin{pmatrix} S_{m-k+1,1} & \cdots & S_{m-k+1,m-k} \\ \vdots & \ddots & \vdots \\ S_{m+n-2k,1} & \cdots & S_{m+n-2k,m-k} \end{pmatrix} \quad (16)$$

$$S_Z(II,II)=\begin{pmatrix} S_{m-k+1,m-k+1} & \cdots & S_{m-k+1,m+n-2k} \\ \vdots & \ddots & \vdots \\ S_{m+n-2k,m-k+1} & \cdots & S_{m+n-2k,m+n-2k} \end{pmatrix} \quad (17)$$

3.3. DERIVATION OF MPTM

By adopting the multi-port network cascading algorithm, sub-matrixes $S_C(I,I)$, $S_C(I,II)$, $S_C(II,I)$, and $S_C(II,II)$ of the MBIA network N_C (in Fig.2) can be calculated based on Eqs. 9 to 12. Most electrical systems involving MBIA have uniform receivers, which means $\Gamma_1=\Gamma_2=\ldots=\Gamma_N=\Gamma$. Thus, calculations can be simplified to yield

$$S_C(I,I)=\Gamma S_A(II,I)(\Delta S)S_A(I,II)+S_A(II,II) \quad (18)$$

$$S_C(I,II)=\Gamma(1+\Gamma)S_A(II,I)(\Delta S)S_A(I,I)+S_A(II,I) \quad (19)$$

$$S_C(II,I)=(1+\Gamma)(\Delta S)S_A(I,II) \quad (20)$$

$$S_C(II,II)=(1+\Gamma)^2(\Delta S)S_A(I,I)+\Gamma U \quad (21)$$

where Γ is the reflection coefficient of the uniform two-port network; U_N is a N ´ N unit matrix and

$$\Delta S=\left(U_N-\Gamma S_A(I,I)\right)^{-1} \quad (22)$$

Based on Eqs. 18–21, termination network N_B contributes to the S-matrix of MBIA network N_C. Hence, we must characterize complete network N_C by considering the effects attributed to N_A and N_B. Since the output ports of the termination network N_B in Fig. 2 are open-circuit, the impedance matrix (Z-matrix) was chosen to represent the complete network N_C. Given N+1 port S-matrix, S_C and its corresponding Z-matrix Z_C can be calculated by

$$Z_C=G_{ref}{}^{-1}(U_{N+1}-S_C)^{-1}(U_{N+1}+S_C)Z_{ref}G_{ref} \quad (23)$$

where U_{N+1} is a N+1 x N+1 unit matrix, and

$$Z_{ref}=Z_0U_{N+1} \quad (24)$$

$$G_{ref}=U_{N+1}/\sqrt{Z_0} \quad (25)$$

where Z_0 is the characteristic impedance and Z_C is related to port voltages and currents in Fig. 1 as:

$$\begin{bmatrix} V_T \\ V_1 \\ \vdots \\ V_N \end{bmatrix}=Z_C\begin{bmatrix} I_T \\ I_1 \\ \vdots \\ I_N \end{bmatrix}=\begin{pmatrix} Z_{TT} & Z_{T1} & \cdots & Z_{TN} \\ Z_{1T} & Z_{11} & \cdots & Z_{1N} \\ \vdots & \vdots & & \vdots \\ Z_{NT} & Z_{N1} & \cdots & Z_{NN} \end{pmatrix}\begin{bmatrix} I_T \\ I_1 \\ \vdots \\ I_N \end{bmatrix} \quad (26)$$

The output ports of MBIA network N_C in Fig. 2 are open-circuit terminated. Thus, we obtain

$$I_1\ I_2\cdots I_N=0 \quad (27)$$

Substituting Eq. 27 into Eq. 26 yields

$$\begin{bmatrix} V_T \\ V_1 \\ \vdots \\ V_N \end{bmatrix}=\begin{bmatrix} Z_{TT}I_T \\ Z_{1T}I_1 \\ \vdots \\ Z_{NT}I_N \end{bmatrix} \quad (28)$$

According to the definition of the transfer function, the MPTM of the MBIA in Fig. 2 can be written as

$$H_C=\begin{bmatrix} V_1/V_T \\ V_2/V_T \\ \vdots \\ V_N/V_T \end{bmatrix}=\begin{bmatrix} Z_{1T}/Z_{TT} \\ Z_{2T}/Z_{TT} \\ \vdots \\ Z_{NT}/Z_{TT} \end{bmatrix} \quad (29)$$

3.4. ANALYSIS AND OPTIMIZATION BASED ON MPTM

In an electrical system involving MBIA, receiver input signals are determined by the spectrum of transmitter output signals and their respective transfer functions, and they are both responsible for meeting specification requirements with sufficient margins. Typical transmitter output signals can be modeled as a series of trapezoid-shaped pulses illustrated in Fig. 5 (see section: supplementary material), where T_{ck} is the system operating the clock period; T_r and T_f are pulse rise and fall time, respectively; T_w is the pulse width; and A_0 is the pulse amplitude. T_w varies depending on the system operating the clock period and system running code. For example, the address/command signals in DDR3 module have various pulse widths in various operations such as single-word, double-word, quad-word, and burst read/write operations.

In Fig. 5 (see section: supplementary material), signals with T_{w1}, T_{w2}, and T_{wn} are designated as 1-, 2-, and n-pattern signals, respectively. The pulse width of the n-pattern signal is given by $T_w = n*T_{ck} - T_r$. A address signal in DDR3 module is taken as example, and it has an operating clock frequency of 667 MHz, rise time T_r of 0.25 ns, fall time T_f of 0.25 ns, and pulse amplitude A0 of 1.5 V. The spectrums of its 1-, 2-, 4-, and 8-pattern signals are calculated in Fig. 6 (see section: supplementary material). The y-axis is the spectrum ratio, which is defined as signal spectrum normalized to the respective DC component. Of the four signals, the 1-pattern signal (solid curve), has the largest spectrum ratio over the entire frequency range shown. This finding means that the 1-pattern signal represents the worst-case scenario and is most critical in designing its transfer characteristic to satisfy the specifications of receiver input signal.

After obtaining the worst-case transmitter output signal in Fig. 6 (see section: supplementary material), the corresponding MPTM represents the transfer characteristic between the transmitter and receivers, and can be used to identify the cause of deterioration of receiver input signal. Loss occurs when the transfer characteristic drops below 0 dB. By contrast, gain occurs when transfer characteristic exceeds 0 dB. The MPTM offers an explicit approach for optimization: an optimized MPTM correlates with an optimized system. The resultant transient worst-case receiver input signals can be predicted by taking IFFT of the spectrum. The result can be assessed if they meet the specification requirements with sufficient margins. Therefore, by employing frequency-domain MPTM as an optimization basis and time-domain transient receiver input signals as assessment, the MBIA can be optimized through effective what-if analysis iterations.

4. RESULT ANALYSIS AND DISCUSSION

4.1. SYSTEM SETUP AND CORRESPONDING MPTM CALCULATIONS

A 22-layer printed circuit board (PCB) with four integrated processing nodes (N_1–N_4) is illustrated in Fig. 7. Each node uses one microprocessor (TMS320C6678 from Texas Instruments) and eight DDR3s (MT41J128M16HA-15EIT from Micron) as external memories. Arbitrary DDR3 address signal in N_1, which links the microprocessor to eight DDR3s, is taken as a case study. U_0 (TMS320C6678) is the transmitter and U_1–U_8 (eight DDR3s) are the receivers. U_1, U_3, U_5, and U_7 are mounted on the top side [Fig.7(a)], and U_2, U_4, U_6, and U_8 are mounted on the bottom [Fig.7(b)].

The link path is designed with fly-by topology as illustrated in Fig. 8 (see section: supplementary material). The parameters are listed in Table I (see section: supplementary material). F_0 denotes the fan-out trace from C6678 and F_1–F_4 denote the fan-out traces from DDR3s. I_1 is the fly-by interval between the C6688 and the first two DDR3s (symmetrical lay-out), and I_2–I_5 are the fly-by intervals between the adjacent DDR3s.

Using the setup in Fig. 8 (see section: supplementary material) and parameters in Table I (see section: supplementary material), a nine-port S-matrix of the link-path network (Eq. 1) was extracted from Mentor Graphics HyperLynx 8.0. U_0 port is the ninth port, whereas U_1–U_8 are the first to eighth ports. The equivalent circuit of the chosen DDR3 address pin was then extracted from its IBIS model (Micron online document) with C_{pkg} = 0.268 pF, L_{pkg} = 1.156 nH, R_{pkg} = 0.1896 ohm, and C_{comp} = 0.625 pF [in Fig. 4(a)]. Based on Eq. 5, the reflection coefficients of the eight two-port networks were calculated. Using Eq. 6, the S-matrix of the termination network were obtained. The reflection coefficients were the same because the receivers were uniform DDR3s. By using the S matrices of the link-path network and termination network, the S-matrix of the MBIA was calculated based on Eqs. 18–21. The MPTM calculated from Eqs. 23–29 is illustrated in Fig. 9, where U_1–U_8 denote the transfer function of DDR3$_1$–DDR3$_8$ and the SFFT (black solid line) denotes the spectrum of the transmitter output signal.

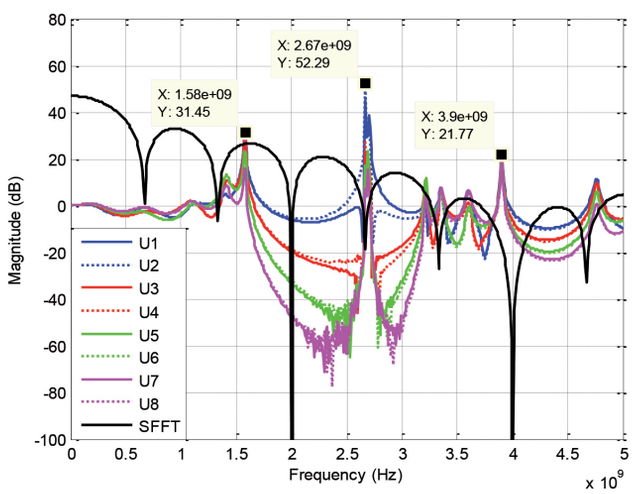

Fig. 9. Calculated MPTM of the multi-branch interconnect architecture

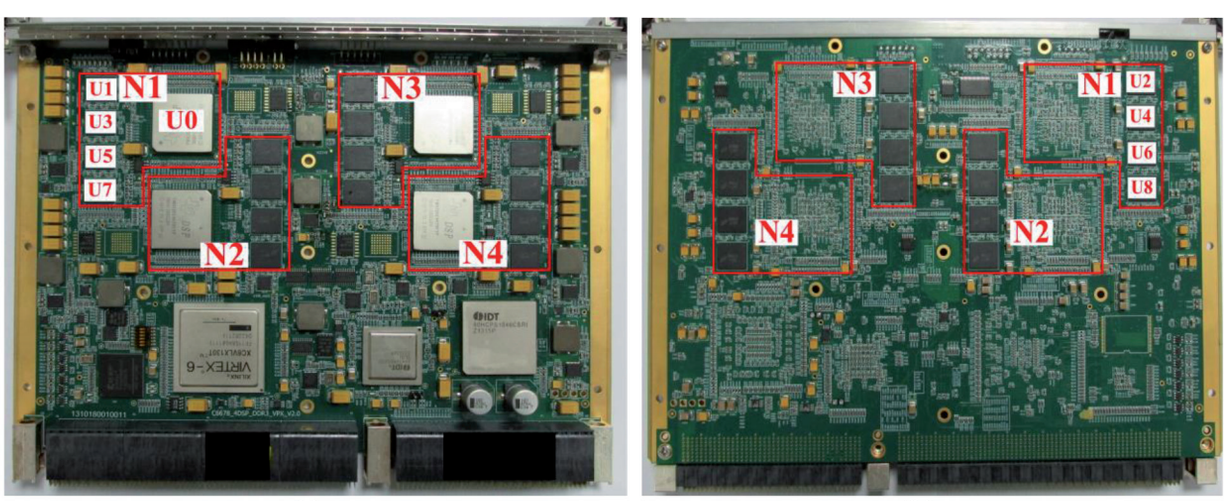

(a) (b)

Fig. 7. A 22-layer PCB with four integrated processing modules (N1–N4): (a) is the board top side, and (b) is the board bottom side

As shown in Fig. 9, the symmetrically placed DDR3s (U_1 and U_2, U_3 and U_4, U_5 and U_6, U_7, and U_8) have almost identical transfer characteristic, which indicates that transient signals at the DDR3s are similar. A close look at transfer functions below 1.3 GHz shows their proximity to 0 dB, which signifies good transfer property for the components of the output signal spectrum of the transmitter. Several pronounced resonances (spikes) occur at frequencies of 1.58 GHz, 2.67 GHz, and 3.9 GHz. These resonances will enhance spectrum components at these frequencies thereby resulting in the corresponding deteriorations of the receiver input signals. Further analysis and optimization based on the MPTM and the worst-case transmitter output signal is demonstrated in the next subsection.

4.2. SIMULATIONS AND DEMONSTRATIONS

In this case study, the worst-case signal output from U_0 (in Fig. 8 (see section: supplementary material)) was taken as the 1-pattern signal with T_r = 0.25 ns, T_f = 0.25 ns, T_w = 1.25 ns, and A_0 = 1.5 V. The FFT of the signal is indicated by the solid black curve in Fig. 9. As shown in Fig. 9, the first resonance of the MPTM curves (U_1–U_8) at around 1.58 GHz is located at one of the peak spectrum components of the black curve. Other resonances (at 2.67 GHz and 3.9 GHz) are located within the valleys of the black curve. Spectrum components in the valley have limited contribution to transient signals at the DDR3s despite high transfer function resonances at 2.67 GHz and 3.9 GHz. Therefore, the fluctuations of the transient signals at the resonance frequency of approximately 1.58 GHz should be expected.

The spectrum of eight DDR3 input signals were calculated using the obtained MPTM and the spectrum of the worst-case transmitter output signal. Next, their respective transient signals were obtained through IFFT, as illustrated by the red star-dotted curves in Fig. 10. Using the same setup and parameters, the transient signals were also generated via simulations in Agilent ADS. The simulated curves (blue solid curves) are shown superimposed on the red star-dotted curves in Fig. 10.

As shown in the Fig. 10, the calculated transient waveforms of DDR3 inputs based on MPTM are consistent with the simulated results from ADS, which verifis the accuracy of the MPTM-based calculation. In addition, the symmetrically designed DDR3s have similar transient signals, which is consistent with the similarity of their transfer characteristics in Fig. 9. All signals in Fig. 10 exhibit fluctuations with a frequency of approximately 1.66 GHz, which correlates with the resonance frequency of 1.58 GHz in Fig. 9 after considering limited accuracy because of sampling points. To confirm this finding, we eliminated the transfer function resonances of U_1, U_3, U_5, and U_7, by forcing transfer function values around 1.58 GHz to 0 dB mathematically. In Fig. 11 (a), the blue solid lines and red dotted lines represent the original and modified transfer functions, respectively. The corresponding transient signals, obtained through IFFT, are shown Fig. 11 (b), where the blue solid lines and red dotted lines are based on the original and modified transfer functions, respectively.

As shown in the Fig. 11, the modification of the transfer function significantly attenuates the magnitude of fluctuation exhibited by the original curves at 1.66 GHz. This finding shows that the first transfer function resonance is primarily responsible for signal deterioration. Therefore, the analysis of the transfer characteristic at the first resonance frequency provides an explicit approach to system optimizations.In practical systems, the MPTM can be optimized by redesigning the link-path parameters in Table I (see section: supplementary material) to attenuate resonances or to move them to the valley spectrum components of the worst-case transmitter output signal (Fig. 9). However, this scenario may not

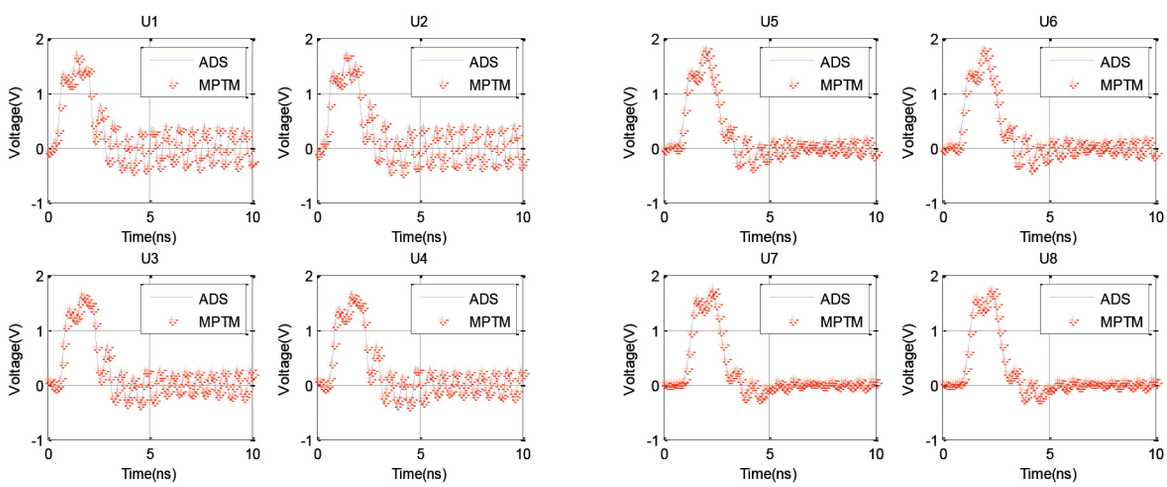

Fig. 10. Transient signals of U1–U8 input. Red star-dotted curves are calculated based on MPTM, whereas the blue solid curves are simulated results from Agilent ADS

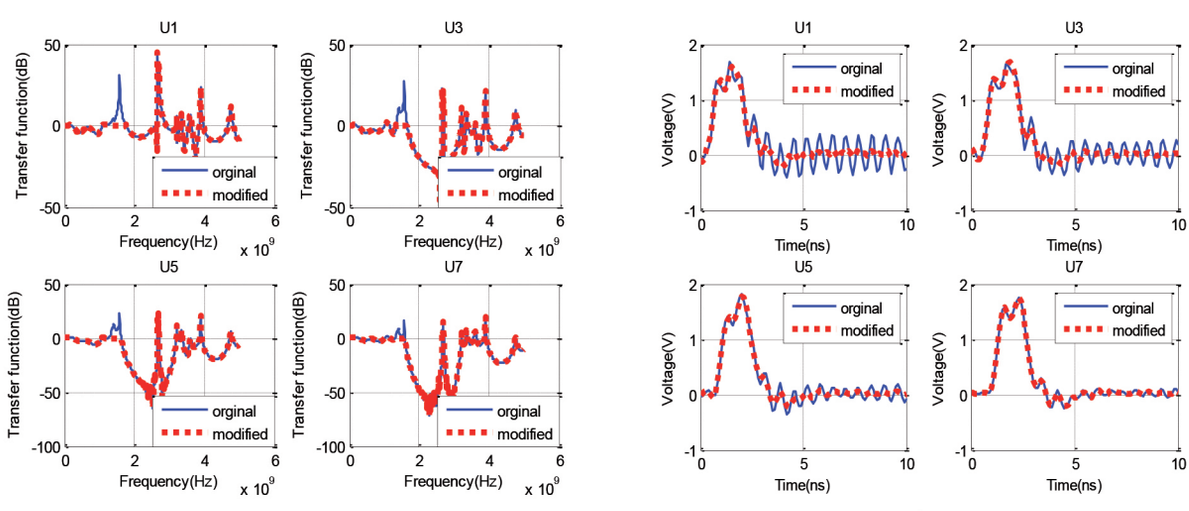

Fig. 11. Transfer characteristics and transient waveforms of U1, U3, U5, and U7: (a) is the orginal and modifed transfer functions, and (b) is the waveforms based on the original and modified transfer functions

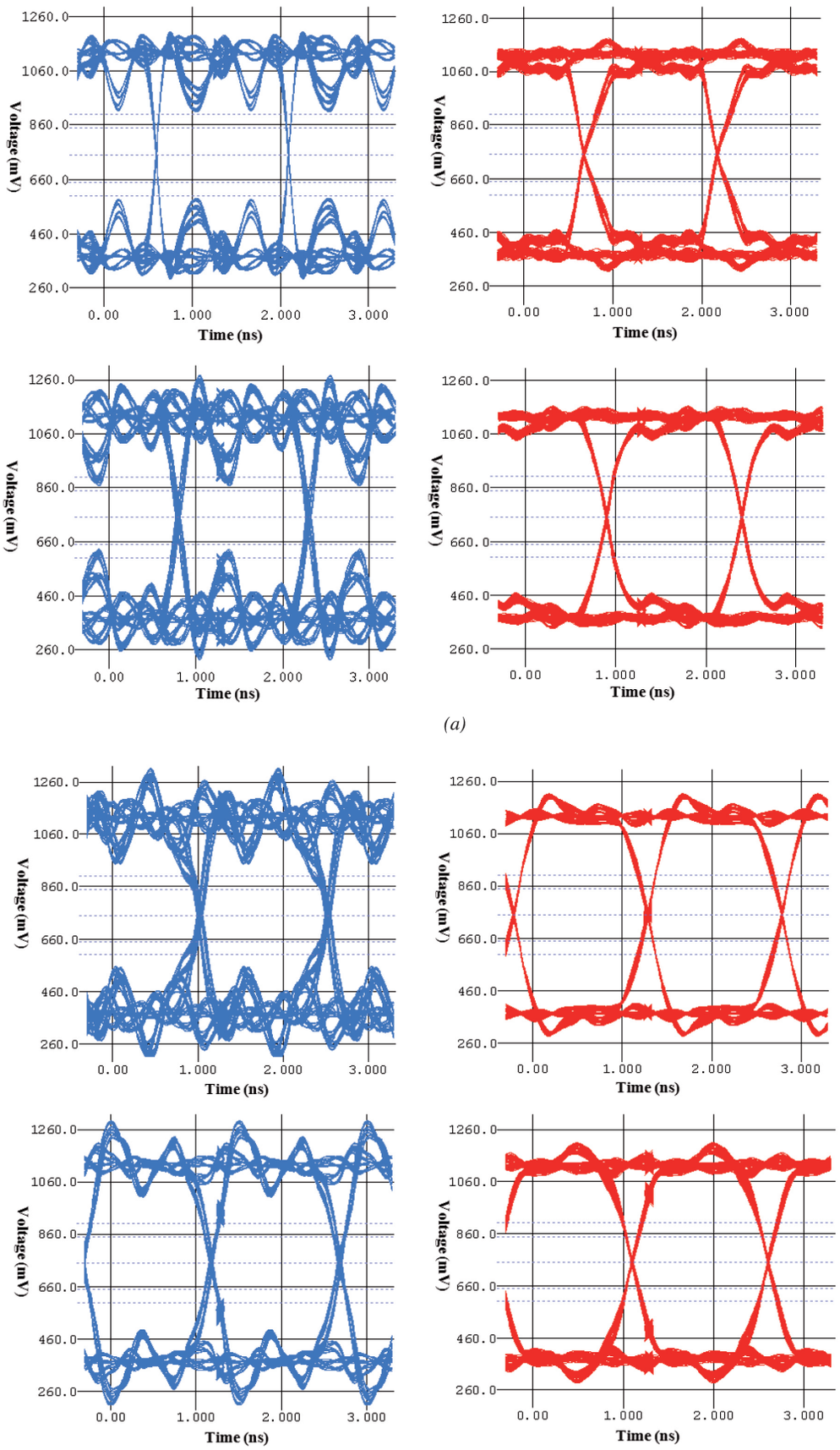

Fig. 12. Eye diagrams of the signals at the input of U1, U3, U5 and U7: (a) illustrates U1 and U3, and (b) illustrates U5 and U7

always be an option because the parameters in Table I (see section: supplementary material) may be fixed due to layout requirements or other constraints.

A practical method is adopted in this study by adding a specific capacitor near the transmitter output. The capacitor is used to attenuate the resonances (1.58 GHz in Fig. 9), and its self-resonance frequency should be near 1.58 GHz for insuring a low impedance to ground. The capacitor should be located to the transmitter output, because the signal components near the 1.58 GHz should be attenuated before it is transmitted across the MBIA, which will greatly enhance these components. Finally, a multi-layer ceramic capacitor was chosen with a capacitance of 7 pf, which was equivalent to series inductance of 20 milliohms and 1.5 nH,whose self-resonance frequency is 1.55GHz (near the 1.58 GHz). With the simuation software of Hyperlynx 8.2 from Mentor Graphics, the overall MBIA including terminations were setup, where the input/output buffere information specification (IBIS) models of the TMS320C6678 from Texas Instruments and MT41J128M16HA-15EIT from Micron were employed. By adding the 7pf capacitor near the transimitter output as the optimization, the overall MBIA was stimulated by pseudo-random binary sequence with bit interval of 1. 5ns. Signal eye diagrams of termination inputs (U_1, U_3, U_5, and U_7) are illustrated in Fig. 12. The blue line in each row represents the eye diagrams before optimization and the red line those after optimization. The quotas of the optimization are listed in Table II.

As shown in Fig. 12 and Table II, the eye height of the DDR3 input signals after optimization increases significantly with an average of 80% and a highest of 139%. Overshoot and undershoot are attenuated, which reduces the risk of chip damage. Although eye width slightly decreases after optimization, which reduces the timing margins, there is sufficient number of margins to satisfy the specification of the DDR3. The results validate the effectiveness and feasibility of the proposed MPTM-based strategy.

DDR No.	Eye Width(ns)			Eye Height (mV)		
	Before Opt	After Opt	Change Rate	Before Opt	After Opt	Change Rate
U1	1.42	1.25	-12%	324	568	75%
U3	1.32	1.32	0%	240	574	139%
U5	1.29	1.27	-2%	396	666	68%
U7	1.3	1.3	0%	506	690	36%

Tabla II. Quotas of the optimization

4. CONCLUSION

To obtain optimal performance and stability of the electrical systems involving MBIA, a novel concept of MPTM was defined to characterize MBIA. MPTM-based strategy was proposed to analyze and optimize the MIBA. An eight-DDR3 address interconnect of fly-by topology was demonstrated. The following are then demonstrated:

(1) MPTM considers termination effects and provides a complete and accurate characterization of electrical systems involving MBIA.

(2) The proposed MPTM-based strategy can identify the causes of signal deterioration and can offer an explicit approach to optimize the system in the frequency domain. The transient receiver input signals can be accurately predicted which enable the signals to be accessed by comparing them to the receiver electrical specifications in the time domain. By combining the two-domain analysis, the system involving MIBA can be optimized by what-if analysis iterations.

(3) The simulation l results show that the proposed strategy can increase the noise margin of the acquired waveforms and can reduce the risk of chip damage caused by overshoot or undershoot.

The present study improved the modeling of MBIA by considering termination effects, and provided an accurate and effective strategy to obtain the optimal performance and stability of electrical systems involving MBIA. However, the limitation continues to exist: termination effects were characterized with low accuracy, and this would leads to an inaccurate MBIA characterization. To overcome this, termination effects modeling should be the focus of future research. Besides, corresponding modeling and simulation software should be developed based on the proposed strategy to facilitate feasible application.

BIBLIOGRAPHY

[1] J. Fan, X. Ye, J. Kim, B. Archambeault, et al. "Signal Integrity Design for High-Speed Digital Circuits: Progress and Directions". IEEE Transactions on Electromagnetic Compatibility. May 2010. Vol. 52- 2. p.392-400. DOI: http://dx.doi.org/10.1109/TEMC.2010.2045381

[2] Stephen H. Hall, Howard L. Heck. "Introduction: The Importance of Signal Integrity". Advanced Signal Integrity for High-Speed Digital Designs. 2009. p.1-8. DOI: http://dx.doi.org/10.1002/9780470423899.ch1

[3] C. R. Paul. Transmission Lines in Digital and Analog Electronic Systems: Signal Integrity and Crosstalk. 2010. p.295-298. DOI: http://dx.doi.org/10.1002/9780470651414.index

[4] T. L. Wu, F. Buesink, F. Canavero. "Overview of Signal Integrity and EMC Design Technologies on PCB: Fundamentals and Latest Progress". IEEE Transactions on Electromagnetic Compatibility. August 2013. Vol. 55-4. p.624-638. DOI: http://dx.doi.org/10.1109/TEMC.2013.2257796

[5] L. Pizano-Escalante, O. Longoria-Gandara, R. Parra-Michel, et al. "Crosstalk Cancellation on High-Speed Interconnects Through a MIMO Linear Precoding". IEEE Transactions on Microwave Theory and Techniques. November 2013. Vol. 61-11. p.3860-3871. DOI: http://dx.doi.org/10.1109/TMTT.2013.2283845

[6] M. S. Zhang, H. Z. Tan, J. F. Mao. "Signal-Integrity Optimization for Complicated Multiple-Input Multiple-Output Networks Based on Data Mining of S-Parameters". IEEE Transactions on Components, Packaging and Manufacturing Technology. July 2014. Vol. 4-7. p.1184-1192. DOI: http://dx.doi.org/10.1109/TCPMT.2014.2306957

[7] B. Ravelo, O. Maurice, S. Lalléchère. "Asymmetrical 1:2 Y-tree interconnects modelling with Kron–Branin formalism". Electronics Letters. July 2016. Vol. 52-14. p.1215-1216. DOI: http://dx.doi.org/10.1049/el.2016.1142

[8] S. Caniggia, F. Maradei. "Comparative Study of Lossy Transmission Line Simulation Models for Eye-Diagram Estimation". IEEE Transactions on Electromagnetic Compatibility. August 2016. Vol. 58-4. p.1176-1183. DOI: http://dx.doi.org/10.1109/TEMC.2016.2538303

[9] N. Maeda, S. Fukui, T. Sekine, Y. Takahashi. "S-parameter estimation for a multiport connection and a multiport device with non-common ground". 2014 International Symposium on Electromagnetic Compatibility. 2014. p.838-843. DOI: http://dx.doi.org/10.1109/EMCEurope.2014.6931020

[10] Paul G. Huray. "Signal Integrity Simulations". The Foundations of Signal Integrity. 2010. p.307-333. DOI: http://dx.doi.org/10.1002/9780470543481.ch8

[11] M. Li, R. Chen. "Method of moments wide-band simulations of the microstrip circuits with second-order Arnoldi reduced model". Electronics Letters. May 2016. Vol. 52-10. p. 841-842. DOI: http://dx.doi.org/10.1049/el.2015.2771

[12] T. Asada, Y. Baba, N. Nagaoka, et al. "An Improved Thin Wire Representation for FDTD Transient Simulations". IEEE Transactions on Electromagnetic Compatibility. June 2015.Vol. 57-3. p. 484-487. DOI: http://dx.doi.org/10.1109/TEMC.2014.2380815

[13] Abderrazak Guettaf, Foued Chabane, Ali Arif, et al. "Dynamic Modeling in a Switched Reluctance Motor SRM using Finite Elements". Journal of Power Technologies. 2013. Vol. 93-3. p.149-153.

[14] Y. Moisiadis, S. Stefanou, P. Papadopoulos." Integrated Inductor Compact Modeling Methodology". Journal of Engineering Science and Technology Review. 2016. Vol. 9- 4. p. 107-110.

[15] Chen Wang, J. L. Drewniak, J. Nadolny. "Anticipating EMI using transfer functions and signal integrity information". 2003 IEEE Symposium on Electromagnetic Compatibility. 2003. Vol.2. p. 695-698. DOI: http://dx.doi.org/10.1109/ISEMC.2003.1236690

[16] M. K. Sampath, N. Atout, "Signal integrity validation of de-embedding techniques using accurate transfer functions". 2012 IEEE 16th International Symposium on Consumer Electronics. 2012. p.1-4. DOI: http://dx.doi.org/10.1109/ISCE.2012.6241710

[17] S. Connor, B. Archambeault, J. C. Diepenbrock. "The impact of external RF energy on high-speed differential signal quality of long cables". 2008 IEEE International Symposium on Electromagnetic Compatibility. 2008. p.1-4. DOI: http://dx.doi.org/10.1109/ISEMC.2008.4652160

[18] R. Jalayer, B. T. Ooi. "Estimation of Electromechanical Modes of Power Systems by Transfer Function and Eigenfunction Analysis". IEEE Transactions on Power Systems. February 2013. Vol. 28-1. p.181-189. DOI: http://dx.doi.org/10.1109/TPWRS.2012.2205279

[19] M. Choi, J. Y. Sim, H. J. Park, et al. "An Approximate Closed-Form Channel Model for Diverse Interconnect Applications". IEEE Transactions on Circuits and Systems I: Regular Papers. October 2014. Vol. 61-10. p.3034-3043. DOI: http://dx.doi.org/10.1109/TCSI.2014.2327275

[20] M. Choi, J. Y. Sim, H. J. Park, et al. "An Approximate Closed-Form Transfer Function Model for Diverse Differential Interconnects". IEEE Transactions on Circuits and Systems I: Regular Papers. May 2015. Vol. 62-5. p.1335-1344. DOI: http://dx.doi.org/10.1109/TCSI.2015.2407435

SUPPLEMENTARY MATERIAL

http://www.revistadyna.com/documentos/pdfs/_adic/8360-1.pdf